# Rigorous Hybrid-Mode Analysis of the Transition from Rectangular Waveguide to Shielded Dielectric Image Guide

JÜRGEN STRUBE AND FRITZ ARNDT, SENIOR MEMBER, IEEE

*Abstract*—**The transition waveguide to shielded and dielectric image guide is analyzed by the rigorous hybrid-mode field expansion technique where higher order mode coupling effects are taken into account directly, also below the corresponding cutoff frequency. The solution of the related eigenvalue problem includes waves with a complex propagation constant although the guide is assumed to be lossless. Calculated diagrams of the propagation constant as a function of frequency, as well as of the permittivity, illustrate the complicated mode conversion between evanescent modes, complex waves, backward waves, and propagating waves. For the three-dimensional scattering problem, the calculated magnitude of the input reflection coefficient agrees well with measurements, whereas the transmission-line theory applied to this structure leads to wrong results.**

## I. Introduction

DIELECTRIC IMAGE GUIDES are finding increasing application for millimeter-wave integrated-circuit designs [1]–[14]. Since rectangular waveguide instrumentation is commonly used in this wavelength range, exact knowledge of the features of the transition to dielectric image guide (Fig. 1), e.g., by means of accurate field-theory methods, is of great importance. This is emphasized by the fact that simple transmission-line theories (cf., e.g., [14]) applied to this discontinuity lead to wrong results. Also, the discussion of the frequency-dependent behavior of this transition may be helpful for further investigations at related discontinuities, like mode launchers [6]–[8], filter structures [10], [12]–[14], or transformer sections [11]. In contrast to the planar dielectric waveguide [19], the step discontinuity shown in Fig. 1 requires all six field components to be considered [23], i.e., in the interpretation of [20] and [12], TE-to-TM (or TM-to-TE) mode coupling has to be taken into account.

Cross-section field and phase constant calculations for this structure have been the subject of many papers, e.g., [1]–[14], including full-wave field expansion analysis [15]–[18]. These investigations, however, are mostly restricted to the dielectric image-guide mode range, where the phase constant $\beta_z$ normalized to the free-space wavenumber $k_0$ is greater than one, and the modes are purely bound to the image guide. Since mode conversion effects [20], [12] occur largely for the range where the modes are not yet purely bound, investigations for normalized propagation constants less than one, as well as for modes below cutoff, may be very informative.

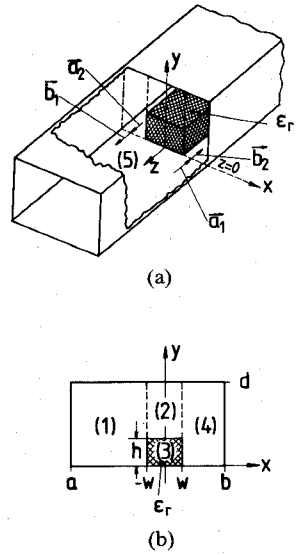


Fig. 1. Shielded dielectric image guide. (a) Transition from rectangular waveguide to shielded dielectric image guide. (b) Cross section.

This paper presents a rigorous hybrid-mode six-field-component analysis of the three-dimensional step discontinuity of Fig. 1. The theory based on expansion of the fields in suitable orthogonal eigenmodes includes the higher order hybrid-mode coupling effects directly. Field matching at the step investigated and normalization to the power carried leads immediately to the interesting scattering coefficients involved. The investigation of the related eigenvalue problem includes backward waves [16] and complex waves [21]–[25]. Since complex wave effects may also be explained as leakage due to mode conversion between constituent waves [20], [12], a profound discussion of the hybrid-mode dispersion behavior, which will include frequency ranges below the cutoff frequency and curves as a function of the permittivity, may help to give further insight to such phenomena. Measurements of the reflection

Manuscript received July 20, 1984; revised January 4, 1985.

The authors are with the Microwave Department, University of Bremen, Kufsteiner Strasse, NW 1, D-2800 Bremen 33, West Germany.

0018-9480/85/0500-0391$01.00 ©1985 IEEE

coefficient at the step discontinuity of Fig. 1 verify the theory for the three-dimensional problem.

## II. Theory

For each subregion $s=1,2,3,4,5$ (Fig. 1), the complete hybrid-mode field is derived from the Hertzian vectors $\vec{P}$ and $\vec{Q}$, respectively, [26]

$$\vec{E}^{(s)}=\nabla\times\nabla\times\vec{P}^{(s)}-j\omega\mu\nabla\times\vec{Q}^{(s)}$$

$$\vec{H}^{(s)}=j\omega\epsilon\nabla\times\vec{P}^{(s)}+\nabla\times\nabla\times\vec{Q}^{(s)}. \tag{1}$$

In (1), TE–TM mode coupling is inherently included. $\vec{P}$ and $\vec{Q}$ are assumed to be sums of suitable eigenmodes satisfying the vector Helmholtz equation and the corresponding boundary conditions

$$\vec{P}^{(s)}=\sum_{\Psi=1}^{psi} h_{\Psi}^{(s)}\cdot\Phi^{(s)}(x,y)\cdot\vec{e}^{(s)}$$

$$\vec{Q}^{(s)}=\sum_{\Psi=1}^{psi} \tilde{h}_{\Psi}^{(s)}\cdot\tilde{\Phi}^{(s)}(x,y)\cdot\vec{e}^{(s)}. \tag{2}$$

For simplicity, in (2), the fields are written at $z=0$ only; the $z$-dependence in forward and backward direction is understood. $h_{\Psi}^{(s)}$ and $\tilde{h}_{\Psi}^{(s)}$ are the still-unknown complex amplitude coefficients of the $\Psi$th mode. The type of modes used for expansion purposes is stated at the end of this section. The expressions for the eigenmodes $\Phi_{\Psi}^{(s)}$ and $\tilde{\Phi}_{\Psi}^{(s)}$ and the relations of the propagation constants in the $z$-direction $\gamma_{z\Psi}^{(s)}$ are given in the Appendix. Note that for the calculations, the vectors $\vec{P}$ and $\vec{Q}$ in (1) are assumed to be $y$-directed in the subregions $s=1,\cdots,4$, and $z$-directed in the subregion $s=5$ (cf. the corresponding unit vector $\vec{e}^{(s)}$ in (A1)–(A5) in the Appendix).

The cross-section eigenvalue problem is treated as in [17], with the exception that an electric wall is considered at $x=a$ (Fig. 1(b)) instead of the one-sided lateral open structure in [17]. Field matching at the boundaries in the $x$, $y$-direction leads to the set of equations for the field amplitudes in (A1)–(A4), which may be written in matrix form

$$(M)\cdot(V)=0 \tag{3}$$

with

$$(V)=\begin{pmatrix} E_k\cdot k_0\cdot\sin\left(\beta_{xk}^{(4)}\cdot(-w-a)\right)\\ F_k\cdot k_0\cdot\cos\left(\beta_{xk}^{(4)}\cdot(-w-a)\right)\\ A_\nu\cdot k_0\cdot k_\nu^{CA}\cdot\sin\left(\beta_{x\nu}^{(2)}\cdot w\right)\\ A'_\nu\cdot k_0\cdot k_\nu^{CA}\cdot\cos\left(\beta_{x\nu}^{(2)}\cdot w\right)\\ B_\mu\cdot k_0\cdot k_\mu^{DB}\cdot\cos\left(\beta_{x\mu}^{(2)}\cdot w\right)\\ B'_\mu\cdot k_0\cdot k_\mu^{DB}\cdot\sin\left(\beta_{x\mu}^{(2)}\cdot w\right)\\ G_k\cdot k_0\cdot\left\{\begin{matrix}\sin\\ \cos\end{matrix}\right\}\left(\beta_{xk}^{(4)}\cdot(w-b)\right)\\ H_k\cdot k_0\cdot\left\{\begin{matrix}\cos\\ \sin\end{matrix}\right\}\left(\beta_{xk}^{(4)}\cdot(w-b)\right)\end{pmatrix}$$

The matrix elements of $(M)$ are given in the Appendix. The propagation constant $\gamma_z$ is calculated by numerical solution of the matrix eigenvalue problem $\det(M)=0$; complex solutions and imaginary values $|\gamma_z|<\omega\sqrt{\mu_0\epsilon_0}$ are included. The complex solutions of $\gamma_z$ of $\det(M)=0$ are advantageously searched with the evolution strategy method [30]. The start value for this direct search process is $\gamma_z=j\beta_z/k_0=j\epsilon_r$, the search range is $j\beta_z/k_0=j\sqrt{\epsilon_r},\cdots,j0$ for the imaginary values, and $\alpha_z/k_0=0,\cdots,7$ for the real values. The relative field amplitudes of the modes are given by the eigenvectors of (3).

By matching the tangential field components at the corresponding interfaces at the step discontinuity at $z=0$ (Fig. 1(a)), the related coefficients $h_\Psi$, $\tilde{h}_\Psi$ of the incident and reflected waves in (2) can be determined by using the orthogonality property of the corresponding eigenmodes. After suitable normalization to the related power leads to the scattering matrix of the step discontinuity at $z=0$ (Fig. 1(a))

$$\begin{pmatrix} b_1\\ b_2\end{pmatrix}=(S)\begin{pmatrix} a_1\\ a_2\end{pmatrix} \tag{4}$$

where $(S)$ is given by

$$(S)=\begin{pmatrix} N_H & & 0\\ & N_E & \\ 0 & & N_\Psi\end{pmatrix}\cdot(W)\begin{pmatrix} N_H & & 0\\ & N_E & \\ 0 & & N_\Psi\end{pmatrix}^{-1} \tag{5}$$

with the normalization coefficients $N$ and the matrix $(W)$ of the wave-amplitude coefficients elucidated in the Appendix.

The convergence behavior of the cross-section eigenvalue problem may be illustrated by plotting the relative field amplitudes against the $x$, $y$ coordinates. Fig. 2(a) shows as

$$(M)=\begin{bmatrix} +HZME_{kk} & +HZMF_{kk} & -HZMRC_{k\nu} & -HZMRS_{k\nu} & -HZMSCS_{k\mu} & +HZMSSS_{k\mu} & 0 & 0\\ -EZME_{kk} & +EZMF_{kk} & -EZMPS_{k\nu} & +EZMPC_{k\nu} & +EZMQSS_{k\mu} & +EZMQCS_{k\mu} & 0 & 0\\ 0 & +HYMF_{kk} & 0 & 0 & -HYMQCS_{k\mu} & +HYMQSS_{k\mu} & 0 & 0\\ +EYME_{kk} & 0 & +EYMTS_{k\nu} & -EYMTC_{k\nu} & 0 & 0 & 0 & 0\\ 0 & 0 & -HZMRC_{k\nu} & +HZMRS_{k\nu} & -HZMSCS_{k\mu} & -HZMSSS_{k\mu} & +HZMG_{kk} & +HZMH_{kk}\\ 0 & 0 & +EZMPS_{k\nu} & +EZMPC_{k\nu} & -EZMQSS_{k\mu} & +EZMQCS_{k\mu} & -EZMG_{kk} & +EZMH_{kk}\\ 0 & 0 & 0 & 0 & -HYMQCS_{k\mu} & -HYMQSS_{k\mu} & 0 & +HYMH_{kk}\\ 0 & 0 & -EYMTS_{k\nu} & -EYMTC_{k\nu} & 0 & 0 & +EYMG_{kk} & 0\end{bmatrix}$$

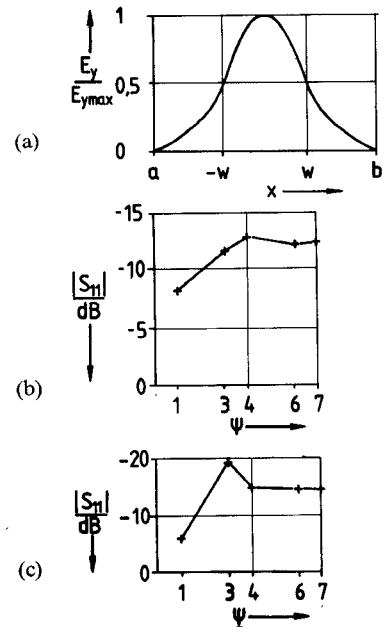


Fig. 2. Illustration of the convergence behavior. (a) Relative field strength $E_y/E_{y\max}$ of the $EH_{11}$ mode along the cross section at $y = 0.1$ d (cf. Fig. 1(b)); $\epsilon_r = 4$, $h = 3.25$ mm, $w = 3.505$ mm, $d = 7.9$ mm, $b = 7.9$ mm, $a = -b$. Number of modes considered $Ny = 7$, cf. (A1)–(A4). (b) Amplitude of the scattering coefficient $S_{11}$ in decibels as a function of the number $\Psi$ of modes considered, cf. (2); $\epsilon_r = 6$, $f = 17.5$ GHz. Dimensions: cf. Fig. 2(a). Mode types considered: 1, 4, 6, 8, 12, 14, and 15 (order of increasing phase-constant values at a fixed frequency). (c) Amplitude of the scattering coefficient $S_{11}$ in decibels as a function of the number $\Psi$ of modes considered; $\epsilon_r = 9$, $f = 16.5$ GHz, $h = 3.2$ mm, $w = 3.45$ mm, $d = 7.9$ mm, $a = -b$. Mode types considered: cf. Fig. 2(b).

an example the $y$-component of the electric field of the fundamental mode versus $x$. Also, by further investigations, we found that with only 11 consecutive modes considered in (2) (cf. Appendix, (A1)–(A4)), no severe discontinuities in the tangential field component along the cross section occur. For the three-dimensional scattering problem, it has turned out to be numerically advantageous to take only those modes in (2) which are excited at the structure under consideration into account. For this purpose, the program checks up the mode-coupling integrals with regard to the exciting $H_{10}$ mode. Zero coupling means that the corresponding mode is not excited; this mode is then omitted from the matching process. In Fig. 2(b) and (c), the convergence behavior of the fundamental $H_{10}$ waveguide mode scattering coefficient $S_{11}$ against the number $\Psi$ of consecutive excited dielectric image-guide modes considered in (2) is shown if an $H_{10}$ wave is incident. Already, for $\Psi = 7$ modes, good convergence may be stated. The dielectric image-guide modes considered for this case are the 1st, 4th, 6th, 8th, 12th, 14th, and 15th modes (order of increasing phase-constant values at a fixed frequency); the related waveguide modes considered are $H_{10}$, $H_{11}$, $H_{31}$, $H_{02}$, $H_{30}$, $E_{11}$, and $E_{31}$.

## III. Results

Fig. 3 shows dispersion curves calculated with this method in comparison with results of [16], [17], and [27]. In order to emphasize the hybrid character of the dielectric

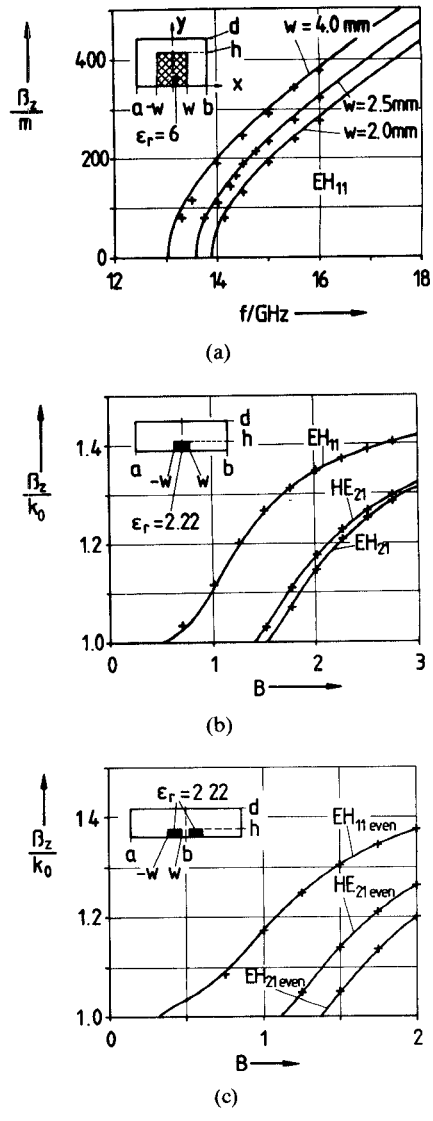


Fig. 3. Calculated dispersion curves in comparison with available results of [16], [17], and [26]. (a) Phase constant $\beta_z$ of the $EH_{11}$ mode versus frequency of a shielded dielectric image guide, with $h = 4.0$ mm, $d = 6.0$ mm, $b = 5.08$ mm, $a = -b$ (+measured results of [16]). (b) Phase constant $\beta_z$ of the first three modes normalized to $k_0 = \omega\sqrt{\mu_0\epsilon_0}$ (free-space wavenumber) versus normalized frequency $B = (4h\sqrt{\epsilon_r - 1})/\lambda_0$ [17] of a "quasi-open" dielectric image guide with $h = 4.1$ mm, $w = 0.99h$, approximated by $b = 10w$, $a = -10w$, $d = 4.8h$ (+calculated results of [17] and [26] for the lateral open structure). (c) Normalized phase constant $\beta_z/k_0$ of the first three even modes versus normalized frequency $B$ of a coupled "quasi-open" dielectric image guide with $h = 4.1$ mm, $w = 1.39h$, $b = 1.51w$ approximated by $a = 7.55w$, and $d = 4.8h$ (electric wall at $x = b$, Fig. 1(a)) (+calculated results of [26] of the lateral open structure).

image-guide modes for normalized phase constants $\beta_z/k_0 \geq 1$ ($k_0 = \omega\sqrt{\mu_0\epsilon_0}$), the designation of [17] is preferred and used throughout the paper: $EH_{mn}$, if the fields associated with the $E$ mode ($E_y$, $E_z$, and $H_z$) are dominant over $E_x$, $H_y$, and $H_z$; for $HE_{mn}$, the reverse is true. The indices $mn$ denote the number of maxima of the $E_y$-components in the dielectric region (3) (cf. Fig. 1(b)) in the $x$- and $y$-direction, respectively. The results calculated with seven consecutive modes in (2) of the shielded (Fig. 3(a)) as well as of the "quasi-open" single image guide (Fig. 3(b), approximated

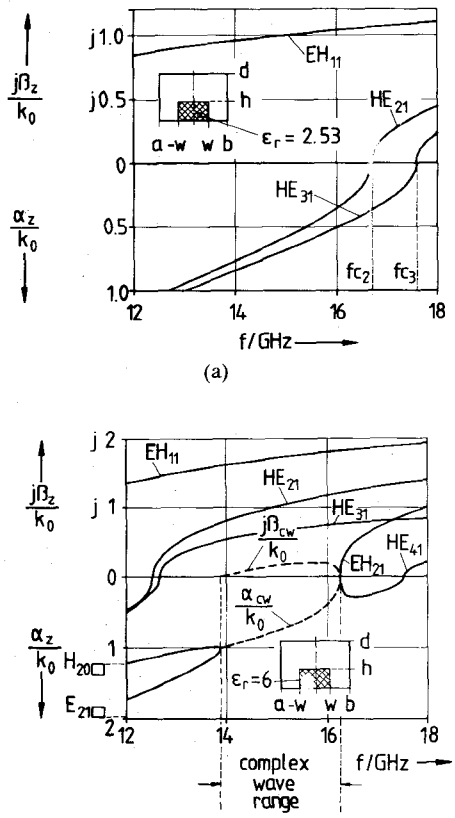


Fig. 4. Propagation constant $\gamma_z = \left\{ \begin{matrix} j\beta_z \\ \alpha_z \end{matrix} \right\}$ normalized with the free-space wavenumber $k_0 = \omega\sqrt{\mu_0\epsilon_0}$ versus frequency of dielectric image line shielded with a conventional rectangular *Ku*-band waveguide housing: 7.899 mm×15.799 mm. (a) Low permittivity $\epsilon_r = 2.53$; $h = 3.15$ mm, $w = 3.505$ mm, $d = 7.9$ mm, $a = -b = -7.899$ mm. (b) Moderately high permittivity $\epsilon_r = 6$, $h = 3.25$ mm, $m = 3.505$ mm, $d = 7.9$ mm, $a = -b = -7.899$ mm. ---- complex waves, propagating with $\exp(\gamma_{cwz} \cdot z)$, where $\gamma_{cwz} = \pm\alpha_{cw} \pm j\beta_{cw}$.

by $b = 10w$, $a = -10w$, $d = 4.8h$ [27]) and coupled image guide (Fig. 3(c), approximated by $a = -7.55w$, $d = 4.8h$ [27], electric wall at $x = b = 1.51w$) agree well with the related values of [16], [17], and [27], respectively. Slight deviations in Fig. 3(b) and (c) may be stated near to the cutoff frequency of the fundamental $EH_{11}$ mode of the two "quasi-open" structures (Fig. 3(b) and (c)) because of the influence of the shield, whereas the real lateral open structure exhibits no low-frequency cutoff. Thus, the comparison with a truly open structure is possi only indirectly. Since the hybrid-mode theory results 17] are already compared in detail with results of othe mmon theories, this comparison is omitted in Fig. 3.

Fig. 4(a) shows the normalized propagation constant $\gamma_z/k_0 = j\beta_z/k_0$ (or $\alpha_z/k_0$, below cutoff) of a dielectric image guide ($\epsilon_r = 2.53$), shielded with a conventional rectangular *Ku*-band waveguide housing.[1] Included is the nonpropagating mode range $\gamma_z/k_0 = \alpha_z/k_0$ below the corresponding cutoff frequencies $f_{c2}, f_{c3}$ of the next higher order modes, $HE_{21}$ and $HE_{31}$, respectively. For simplicity, the corresponding real $\alpha_z$ values are plotted in the same diagram, like e.g., in [29], but, for lucidity, in the opposite direction. For low permittivity ($\epsilon_r = 2.53$, Fig. 4(a)), standard dispersion behavior can be stated and the unique fundamental $EH_{11}$-mode propagation extends nearly the whole *Ku*-band frequency range. Already, for moderately high permittivity ($\epsilon_r = 6$, Fig. 4(b)), however, between 13.9 and 16.3 GHz, the eigenvalue solution of Section II leads to a complex propagation constant $\gamma_{cwz} = \pm\alpha_{cw} \pm j\beta_{cw}$, in spite of the assumption that the shielded dielectric image guide is lossless. This apparent contradiction may be resolved by interpretation of calculated lines of real power flow [25], [24], supported by a "complex" mode [21] or wave [22], which indicate power transmission with opposite signs: in the forward direction inside the dielectric region, in the backward direction outside, or vice versa. The affinity to the leakage effects stated by [20] and [12] is obvious. The total power transmitted by a complex wave through the total cross section of the shielded dielectric image guide is zero, although a real power flow exists. Moreover, for complex waves, the orthogonality relation still holds [25].

In Fig. 4(b), below the cutoff frequency, the higher order $EH_{21}$ mode degenerates to a pair of complex waves propagating in the $\pm z$-direction with $j\beta_{cw}$, and the attenuation constant is $\alpha_{cw}$. For still lower frequencies, the complex waves split into two evanescent modes. The corresponding rectangular waveguide mode propagation constants calculated for the ordinate (in Fig. 4(b) at 12 GHz) may suggest a certain affinity to the pure waveguide $H_{20}$ and $E_{21}$ modes. The actual mode conversion, however, is more complicated.

Fig. 5, where the normalized propagation constant $\gamma_z/k_0 = \{j\beta_z/k_0;\ \alpha_z/k_0\}$ is plotted against the permittivity $\epsilon_r$, allows the modes to be assigned directly to rectangular waveguide modes ($\epsilon_r = 1$) at finite frequencies ($f = 5$ GHz, Fig. 5(a); $f = 14$ GHz, Fig. 5(b)); nevertheless, the plots against $\epsilon_r$ may be considered as (slightly distorted) dispersion curves, since increasing permittivity corresponds to a nonlinear frequency scale. Moreover, all typical results are verified by a real frequency scale (cf., e.g., Fig. 7).

The results of Fig. 5(a) may be summarized as follows. 1) Three complex waves cover nearly the whole indicated permittivity range. 2) The fundamental $EH_{11}$ mode already degenerates to a pair of complex waves (complex wave 2). 3) Evanescent modes may convert to complex waves, which may lead to propagating modes (complex wave 2). 4) Evanescent modes may convert to complex waves, which may lead to backward waves (complex wave 2). 5) Evanescent modes may convert to complex waves, which may lead to evanescent modes (complex wave 3). 6) Waveguide modes may convert directly to complex waves (complex wave 1). 7) There are backward evanescent modes (between the complex waves 1 and 2). 8) There are new types of evanescent modes designated as $HE_{20-01}$ and $HE_{20+01}$ modes; the $HE_{20-01}$ mode yields a field concentration within the dielectric region (cf. Fig. 6(a)) and leads directly to the propagating $HE_{21}$ mode—the contrary is true for the $HE_{20+01}$ mode (cf. Fig. 6(b)), which remains an

[1] 15.799 mm×7.899 mm (12.4–18 GHz).

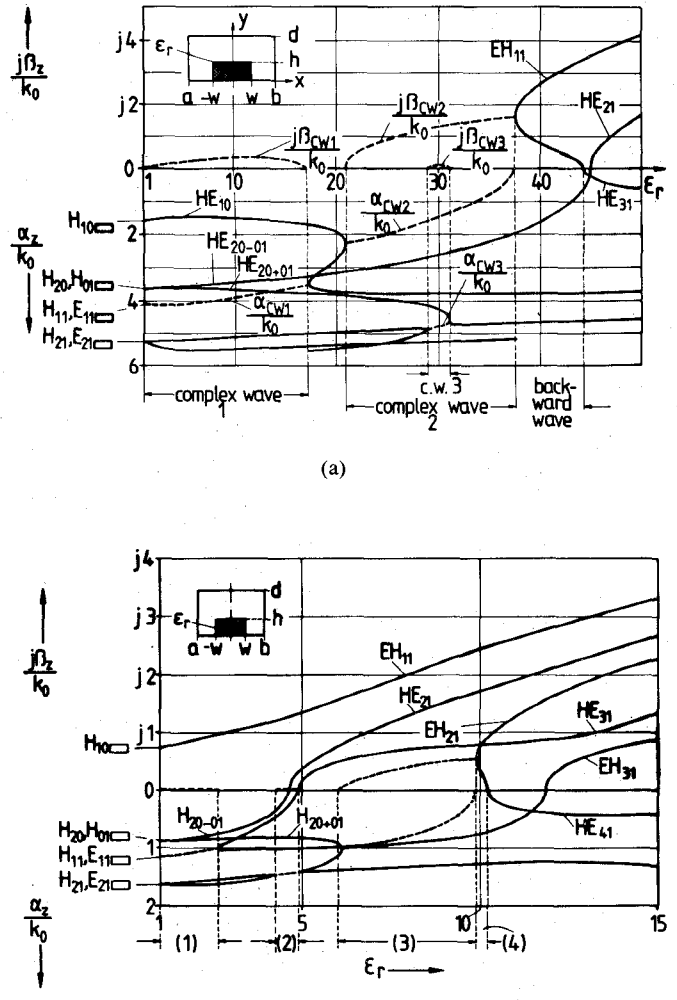


Fig. 5. Propagation constant $\gamma_z = \begin{Bmatrix} j\beta_z \\ \alpha_z \end{Bmatrix}$ normalized with the free-space wavenumber $k_0 = \omega\sqrt{\mu_0\epsilon_0}$ plotted against permittivity $\epsilon_r$ of a dielectric image line shielded with a conventional *Ku*-band waveguide housing: 7.899 mm × 15.799 mm. (a) Frequency $f = 5$ GHz ($a = -b = -7.899$ mm, $w = 3.45$ mm, $h = 3.2$ mm, $d = 7.9$ mm). ---- complex wave. (b) Frequency $f = 14$ GHz (same dimensions as Fig. 5(a)). ---- complex wave, (1) complex wave 1, (2) complex wave 2, (3) complex wave 3, (4) backward wave.

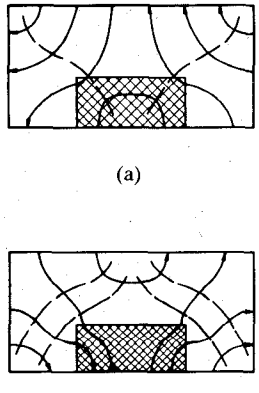


Fig. 6. Field of evanescent modes at $\epsilon_r = 5$, $f = 5$ GHz, indicated in Fig. 5(a). (a) $H_{20-01}$ mode leading to the $HE_{21}$ propagating mode. (b) $H_{20+01}$ remaining evanescent mode ($E_z$, $H_z$ not shown).

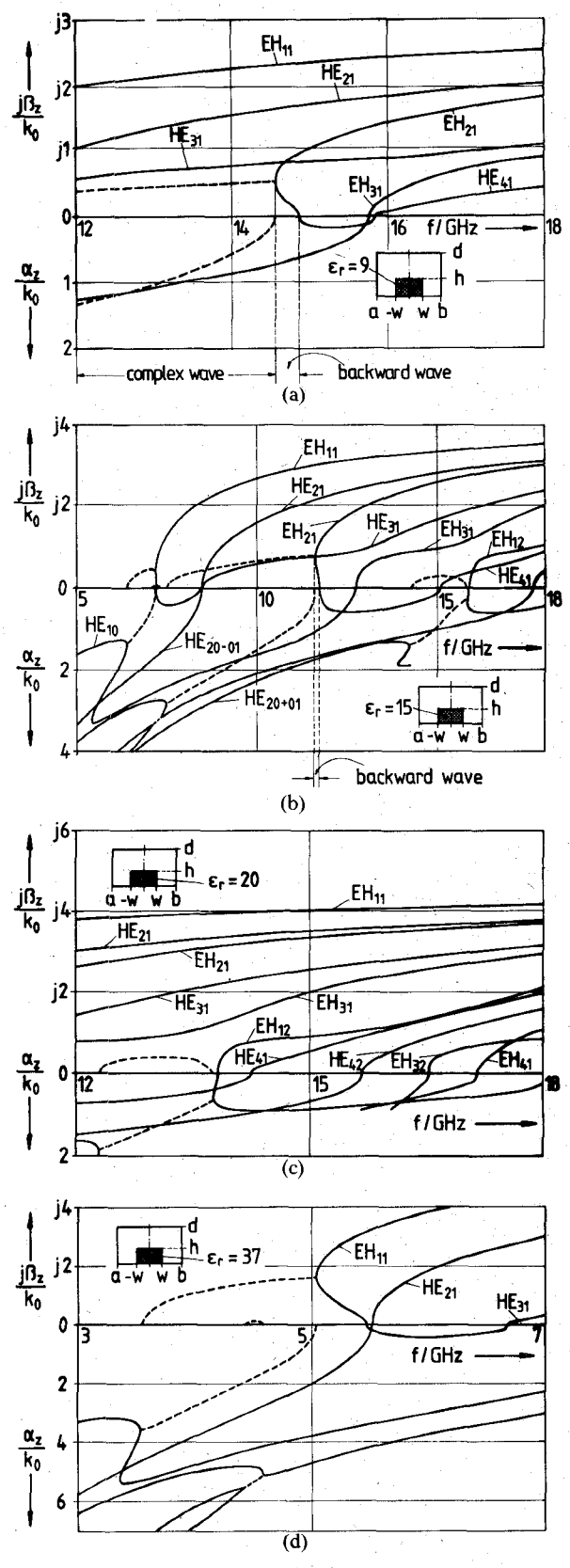


Fig. 7. Propagation constant $\gamma_z = \begin{Bmatrix} j\beta_z \\ \alpha_z \end{Bmatrix}$ normalized with the free-space wavenumber $k_0 = \omega\sqrt{\mu_0\epsilon_0}$ versus frequency; dielectric image line shielded with a conventional *Ku*-band waveguide housing: 7.899 mm × 15.799 mm. (a) $\epsilon_r = 9$; $h = 3.2$ mm, $w = 3.45$ mm, $d = 7.899$ mm, $b = 7.899$ mm, $a = -b$. ---- complex wave, bw: backward wave. (b) $\epsilon_r = 15$, dimensions: cf. Fig. 7(a). ---- complex wave, bw: backward wave. (c) $\epsilon_r = 20$. (d) $\epsilon_r = 37$.

evanescent mode. 9) The $H_{10}$ waveguide mode enlarged by a $E_z$-component ($HE_{10}$ mode) splits in complex waves (complex wave 2, which converts to the fundamental $EH_{11}$ mode) and in a backward evanescent mode. 10) The fundamental $EH_{11}$ mode (which may be considered to be constituted by the fundamental $H_{10}$ waveguide mode via the complex wave 2) is combined with the higher order $HE_{31}$ mode (showing even symmetry like the $EH_{11}$ mode) via a backward wave; this may visualize the close affinity between these modes. Additionally, it should be noted that complex waves exist in the evanescent mode range of the corresponding propagating waves; the cutoff frequencies of propagating higher order modes are no reliable criterion for the absence of leakage affects [12], which may be caused by complex waves, especially since the fundamental $EH_{11}$ mode may already degenerate to complex waves below its cutoff frequency.

In Fig. 5(b), where the fundamental $EH_{11}$ mode is above its cutoff frequency, analogous results to Fig. 5(a) may be perceived. The complex wave 3) and the backward wave 4) may be considered as original parts of the higher order mode pair $HE_{41}$ and $EH_{21}$. Fig. 6(a) and (b) shows the evanescent $H_{20-01}$ and $H_{20+01}$ mode fields (at $\epsilon_r = 5$, Fig. 5(a)) already mentioned above (statement 8)).

Fig. 7 exhibits the dispersion curves—propagation constant $\gamma_z$ normalized with the free-space wavenumber $k_0 = \omega\sqrt{\mu_0\epsilon_0}$ as a function of frequency—for the dielectric image line shielded with a *Ku*-band waveguide housing for several permittivity values ($\epsilon_r$ as a parameter). The analogy to the corresponding curves (Fig. 5) as a function of permittivity at fixed frequencies is obvious and the related statements still hold. Fig. 7(a), for instance, indicates again that complex waves may occur below the cutoff frequency of the corresponding propagating modes to which they are constituent parts.

Fig. 8 shows the magnitude of the scattering coefficients $S_{11}$ at the step-discontinuity rectangular waveguide to the shielded dielectric image guide (Fig. 1(a)) if a $H_{10}$ ($TE_{10}$) wave is incident. The magnitude of $S_{11}$, which is relatively easy to measure—opposite to the phase angle, especially for all cases of simultaneous higher order mode propagation—has turned out to be an adequate criterion to verify the theory. The hybrid-mode analysis results (solid line) are compared with measurements and with results of transmission-line theory (cf., e.g., [14]) applied to this structure. Only for $\epsilon_r = 2.53$ (Fig. 8(a)) does the transmission-line theory lead to satisfactory agreement with the hybrid-mode analysis. This may be illustrated by Fig. 4(a), where for nearly the whole *Ku*-band (12.4–18 GHz) only the fundamental $EH_{11}$ mode propagates. For higher permittivity, $\epsilon_r = 6$ (Fig. 8(a)), $\epsilon_r = 9$ (Fig. 8(b)), and $\epsilon_r = 20$ (Fig. 8(c)); however, these examples indicate that the hybrid-mode analysis results (calculated by only seven consecutive modes selected by the criterion of excitation by the incident $H_{10}$ mode; cf. Fig. 2(b) and (c)) agree well with measurements, whereas the transmission-line theory leads to wrong results.

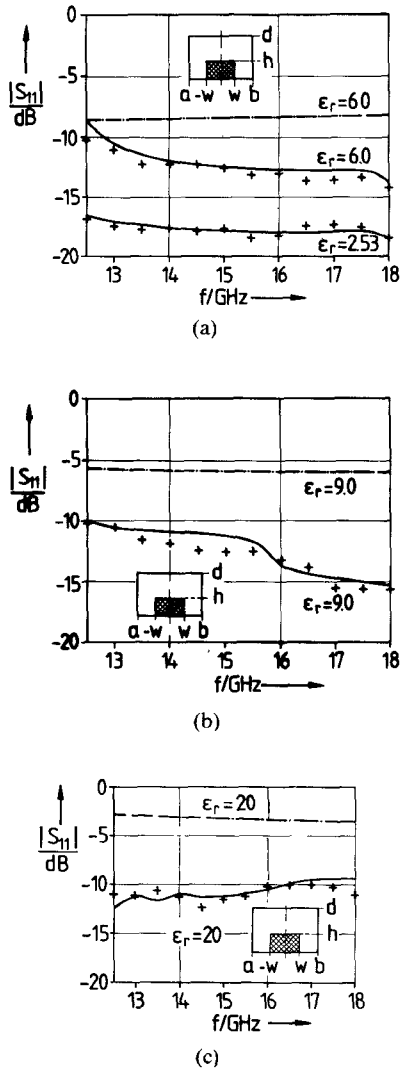


Fig. 8. Magnitude of the scattering coefficient $S_{11}$ at the step discontinuity rectangular waveguide to shielded dielectric image guide if a $H_{10}$ ($TE_{10}$) wave is incident. —— calculated with the hybrid-mode analysis. ----- calculated by transmission-line theory (cf., e.g., [14]). + + + + + measured. (a) $\epsilon_r = 2.53$, $h = 3.15$ mm, and $\epsilon_r = 6$, $h = 3.25$ mm, $w = 3.505$ mm, $d = 7.899$ mm, $b = 7.899$ mm, $a = -b$. (For $\epsilon_r = 2.53$, the transmission-line theory results are nearly identical with those of the hybrid-mode analysis and are, therefore, omitted.) (b) $\epsilon_r = 9$, $h = 3.2$ mm, $w = 3.45$ mm, $d = 7.899$ mm, $b = 7.899$ mm, $a = -b$. (c) $\epsilon_r = 20$, $h = 3.2$ mm, $w = 3.45$ mm, $d = 7.899$ mm, $b = 7.899$ mm, $a = -b$.

## IV. Conclusion

A rigorous hybrid-mode analysis of the transition from rectangular waveguide to shielded dielectric image guide is described. Based on expansion of the fields in suitable orthogonal eigenmodes, the theory takes into account higher order hybrid-mode coupling effects directly, also below the corresponding cutoff frequency. The investigation of the related eigenvalue problem, in addition to backward waves, includes frequency ranges where the propagation constant is complex in spite of the assumption that the guide be lossless. These complex waves exhibit power transmission with opposite signs: in the forward direction inside the dielectric region, in the backward direction outside, or vice

versa. The affinity to leakage effects, stated recently, is obvious. Calculated diagrams of the propagation constant as a function of frequency, as well as of the permittivity, indicate that complex waves occur nearly over the whole investigated range. Some important results may be summarized as follows: the fundamental mode already degenerates to a pair of complex waves; evanescent modes may convert to complex waves, which may lead to propagating modes, backward waves, or again to evanescent modes; waveguide modes may convert directly to complex waves; there are backward evanescent modes and evanescent modes which may be considered to be sums or differences of degenerated waveguide modes; complex waves exist in the evanescent mode range of the corresponding propagating waves; therefore, the cutoff frequencies are no reliable criterion for the absence of leakage effects caused by complex waves, especially since the fundamental mode may already degenerate to complex waves. For the three-dimensional scattering problem of the transition waveguide to shielded image guide, the magnitude of the input reflection coefficient calculated with only seven consecutive excited modes agrees well with measurements, whereas the transmission-line theory applied to this structure leads to wrong results.

## APPENDIX

### A. Eigenmode Expressions for (2)

$s = 1$:

$$\Phi_\Psi^{(1)}(x,y) = \sum_{\nu=1}^{Ny} E_\nu \sin\left(\beta_{x\nu}^{(4)}(x-a)\right)\cos\beta_{y\nu}^{(4)} y$$

$$\tilde{\Phi}_\Psi^{(1)}(x,y) = \sum_{\mu=1}^{My} F_\mu \cos\left(\tilde{\beta}_{x\mu}^{(4)}(x-a)\right)\sin\tilde{\beta}_{y\mu}^{(4)} y$$

$$\vec{e}^{(1)} = \vec{e}_y; \qquad \tilde{h}_\Psi^{(1)} = h_\Psi^{(1)} = h_\Psi^{(2\cdots 4)} = \tilde{h}_\Psi^{(2\cdots 4)} \tag{A1}$$

$s = 2$:

$$\Phi_\Psi^{(2)}(x,y) = \sum_{\nu=1}^{Ny} \left(A_\nu \sin\beta_{x\nu}^{(2)} x + A'_\nu \cos\beta_{x\nu}^{(2)} x\right) \cdot \cos\beta_{y\nu}^{(2)}(y-d)$$

$$\tilde{\Phi}_\Psi^{(2)}(x,y) = \sum_{\mu=1}^{My} \left(B_\mu \cos\tilde{\beta}_{x\mu}^{(2)} x + B'_\mu \sin\tilde{\beta}_{x\mu}^{(2)} x\right) \cdot \sin\left(\tilde{\beta}_\mu^{(2)}(y-d)\right)$$

$$\vec{e}^{(2)} = \vec{e}_y; \qquad h_\Psi^{(2)} = \tilde{h}_\Psi^{(2)} = h_\Psi^{(1)} = \tilde{h}_\Psi^{(1)} = h_\Psi^{(3,4)} = \tilde{h}_\Psi^{(3,4)} \tag{A2}$$

$s = 3$:

$$\Phi_\Psi^{(3)}(x,y) = \sum_{\nu=1}^{Ny} \left(C_\nu \sin\beta_{x\nu}^{(2)} x + C'_\nu \cos\beta_{x\nu}^{(2)} x\right)\cos\beta_{y\nu}^{(3)} y$$

$$\tilde{\Phi}_\Psi^{(3)}(x,y) = \sum_{\mu=1}^{My} \left(D_\mu \cos\tilde{\beta}_{x\mu}^{(2)} + D'_\mu \sin\tilde{\beta}_{x\mu}^{(2)} x\right)\sin\tilde{\beta}_{y\mu}^{(3)} y$$

$$\vec{e}^{(3)} = \vec{e}_y; \qquad h_\Psi^{(3)} = \tilde{h}_\Psi^{(3)} = h_\Psi^{(1,2)} = \tilde{h}_\Psi^{(1,2)} = h_\Psi^{(4)} = \tilde{h}_\Psi^{(4)} \tag{A3}$$

$s = 4$:

$$\Phi_\Psi^{(4)}(x,y) = \sum_{\nu=1}^{Ny} G_\nu \sin\beta_{x\nu}^{(4)}(x-b)\cos\beta_{y\nu}^{(4)} y$$

$$\tilde{\Phi}_\Psi^{(4)}(x,y) = \sum_{\mu=1}^{My} H_\mu \cos\left(\tilde{\beta}_{x\mu}^{(4)}(x-b)\right)\sin\tilde{\beta}_{y\mu}^{(4)} y$$

$$\vec{e}^{(4)} = \vec{e}_y; \qquad h_\Psi^{(4)} = \tilde{h}_\Psi^{(4)} = h_\Psi^{(1\cdots 3)} = \tilde{h}_\Psi^{(1\cdots 3)} \tag{A4}$$

$s = 5$:

$$\Phi_\Psi^{(5)}(x,y) = \sin\left(\frac{m\pi}{(b-a)}\cdot(x-a)\right)\sin\frac{n\pi}{d} y$$

$$\tilde{\Phi}_\Psi^{(5)}(x,y) = \cos\left(\frac{m\pi}{(b-a)}(x-a)\right)\cos\frac{n\pi}{d} y$$

$$\vec{e}^{(5)} = \vec{e}_z, \Psi = m,n. \tag{A5}$$

(By this choice, a unique assignment to the waveguide $E$ and $H$ modes is possible.)

### B. Relations for the Propagation Constants

$$\beta_{y\nu}^{(4)} = \frac{\nu\cdot\pi}{d}, \qquad \nu = 0,1,2,\cdots$$

$$\tilde{\beta}_{y\mu}^{(4)} = \frac{\mu\pi}{d}, \qquad \mu = 1,2,3,\cdots \tag{A6}$$

$$k_0^2 = \omega^2\mu_0\epsilon_0$$

$$k_0^2 = -\gamma_z^2 + \beta_{x\nu}^{(4)2} + \beta_{y\nu}^{(4)2} = -\gamma_z^2 + \tilde{\beta}_{x\mu}^{(4)2} + \tilde{\beta}_{y\mu}^{(4)2}$$

$$k_0^2 = -\gamma_z^2 + \beta_{x\nu}^{(2)2} + \beta_{y\nu}^{(2)2} = -\gamma_z^2 + \tilde{\beta}_{x\mu}^{(2)2} + \tilde{\beta}_{y\mu}^{(2)2}$$

$$k_0^2\cdot\epsilon_r^{(3)} = -\gamma_z^2 + \beta_{x\nu}^{(3)2} + \beta_{y\nu}^{(3)2} = -\gamma_z^2 + \tilde{\beta}_{x\mu}^{(3)2} + \tilde{\beta}_{y\mu}^{(3)2} \tag{A7}$$

$$\beta_{y\nu}^{(3)}\cdot\sin\left(\beta_{y\nu}^{(3)}h\right)\cos\left(\beta_{y\nu}^{(2)}(h-d)\right) - \epsilon_r^{(3)}\beta_{y\nu}^{(2)}\cos\left(\beta_{y\nu}^{(3)}h\right)\cdot\sin\left(\beta_{y\nu}^{(2)}(h-d)\right) = 0 \tag{A8}$$

$$\cos\left(\tilde{\beta}_{y\mu}^{(2)}(h-d)\right)\sin\left(\tilde{\beta}_{y\mu}^{(3)}h\right) - \frac{\tilde{\beta}_{y\mu}^{(3)}}{\tilde{\beta}_{y\mu}^{(2)}}\cdot\cos\left(\tilde{\beta}_{y\mu}^{(3)}\right)\cdot\sin\left(\tilde{\beta}_{y\mu}^{(2)}(h-d)\right) = 0. \tag{A9}$$

### C. Matrix Elements of (3)

$$HZME_k = \omega\epsilon_0\cdot\frac{d}{2}\cdot N_k\cdot\frac{\beta_{xk}^{(4)}\cdot\cos\left(\beta_{xk}^{(4)}\cdot(-w-a)\right)}{k_0\cdot\sin\left(\beta_{xk}^{(4)}\cdot(-w-a)\right)}$$

$$HZMF_k = \frac{k\pi}{2}\cdot\frac{-j\gamma_z}{k_0}$$

$$HZMRC_{k\nu} = \omega\epsilon_0\cdot\frac{\beta_{x\nu}^{(2)}\cdot R_{k\nu}\cdot\cos\left(\beta_{x\nu}^{(2)}\cdot(-w)\right)}{k_0\cdot k_\nu^{CA}\cdot\sin\left(\beta_{x\nu}^{(2)}\cdot(+w)\right)}$$

$$\pm HZMRS_{k\nu} = \omega\epsilon_0\cdot\frac{\beta_{x\nu}^{(2)}\cdot R_{k\nu}\cdot\sin\left(\beta_{x\nu}^{(2)}\cdot(\pm w)\right)}{k_0\cdot k_\nu^{CA}\cdot\cos\left(\beta_{x\nu}^{(2)}\cdot(+w)\right)}$$

$$HZMSCS_{k\mu} = \frac{-j\gamma_z\cdot S_{k\mu}}{k_0\cdot k_\mu^{DB}}$$

$$\pm HZMSSS_{k\mu} = \pm\frac{-j\gamma_z\cdot S_{k\mu}}{k_0\cdot k_\mu^{DB}} \tag{A10}$$

$$EZME_k = \frac{k\pi}{2}\cdot\frac{-j\gamma_z}{k_0}$$

$$EZMF_k = \omega\mu_0\cdot\frac{d}{2}\cdot\frac{\beta_{xk}^{(4)}\cdot\sin\left(\beta_{xk}^{(4)}\cdot(-w-a)\right)}{k_0\cdot\cos\left(\beta_{xk}^{(4)}\cdot(-w-a)\right)}$$

$$\pm EZMPS_{k\nu} = \pm\frac{-j\gamma_z\cdot P_{k\nu}}{k_0\cdot k_\nu^{CA}}$$

$$EZMPC_{k\nu} = \frac{-j\gamma_z\cdot P_{k\nu}}{k_0\cdot k_\nu^{CA}}$$

$$\pm EZMQSS_{K\mu} = \omega\mu_0\cdot\frac{\tilde\beta_{x\mu}^{(2)}\cdot Q_{k\mu}\cdot\sin\left(\tilde\beta_{x\mu}^{(2)}\cdot(\pm w)\right)}{k_0\cdot k_\mu^{DB}\cdot\cos\left(\tilde\beta_{x\mu}^{(2)}\cdot(+w)\right)}$$

$$EZMQCS_{k\mu} = \omega\mu_0\cdot\frac{\tilde\beta_{x\mu}^{(2)}\cdot Q_{k\mu}\cdot\cos\left(\tilde\beta_{x\mu}^{(2)}\cdot(-w)\right)}{k_0\cdot k_\mu^{DB}\cdot\sin\left(\tilde\beta_{x\mu}^{(2)}\cdot(+w)\right)} \tag{A11}$$

$$HYMF_k = \frac{d}{2}\cdot\frac{\left[\beta_{xk}^{(4)^2}-\gamma_z^2\right]}{k_0}$$

$$HYMQCS_{k\mu} = \frac{\left[\beta_{x\mu}^{(2)^2}-\gamma_z^2\right]\cdot Q_{k\mu}}{k_0\cdot k_\mu^{DB}}$$

$$\pm HYMQSS_{k\mu} = \pm\frac{\left[\beta_{x\mu}^{(2)^2}-\gamma_z^2\right]\cdot Q_{k\mu}}{k_0\cdot k_\mu^{DB}} \tag{A12}$$

$$EYME_k = \frac{d}{2}\cdot N_k\cdot\frac{\left[\beta_{xk}^{(4)^2}-\gamma_z^2\right]}{\beta_0}$$

$$\pm EYMTS_{k\nu} = \pm\frac{\left[\beta_{x\nu}^{(2)^2}-\gamma_z^2\right]\cdot T_{k\nu}}{\beta_0\cdot k_\nu^{CA}}$$

$$EYMTC_{k\nu} = \frac{\left[\beta_{x\nu}^{(2)^2}-\gamma_z^2\right]\cdot T_{k\nu}}{\beta_0\cdot k_\nu^{CA}}$$

$$EYMG_k = \frac{d}{2}\cdot N_k\cdot\frac{\left[\beta_{xk}^{(4)^2}-\gamma_z^2\right]}{\beta_0} \tag{A13}$$

$$HYMH_k = \frac{d}{2}\cdot\frac{\left[\beta_{xk}^{(4)^2}-\gamma_z^2\right]}{\beta_0}$$

$$EZMG_k = \frac{k\pi}{2}\cdot\frac{-j\gamma_z}{\beta_0} \tag{A14}$$

$$EZMH_k = \omega\mu_0\cdot\frac{d}{2}\cdot\frac{\beta_{xk}^{(4)}\cdot\left\{\begin{matrix}\sin\\ \cos\end{matrix}\right\}\left(\beta_{xk}^{(4)}\cdot(w-b)\right)}{k_0\cdot\left\{\begin{matrix}\cos\\ \sin\end{matrix}\right\}\left(\beta_{xk}^{(4)}\cdot(w-b)\right)}$$

$$HZMG_k = \omega\epsilon_0\cdot\frac{d}{2}\cdot N_k\cdot\frac{\beta_{xk}^{(4)}\cdot\left\{\begin{matrix}\cos\\ \sin\end{matrix}\right\}\left(\beta_{xk}^{(4)}\cdot(w-b)\right)}{k_0\cdot\left\{\begin{matrix}\sin\\ \cos\end{matrix}\right\}\left(\beta_{xk}^{(4)}\cdot(w-b)\right)}$$

$$HZMH_k = \frac{k\pi}{2}\cdot\frac{-j\gamma_z}{k_0}. \tag{A15}$$

### D. Normalization Coefficients of (5)

$$N_{Hmn} = \pm\tilde h_{mn}^{(5)} + \sqrt{\omega\mu_0\beta_{zmn}^{(5)}\frac{(b-a)}{4}d\left[\left(\frac{m\cdot\pi}{b-a}\right)^2\cdot N_n+\left(\frac{n\cdot\pi}{d}\right)N_m\right]}$$

$N_k$ = Neumann-factor, $\begin{pmatrix}N=2 & \text{for } k=0\\ N=1 & \text{for } k\neq 0\end{pmatrix}$

$$N_{Emn} = \pm h_{mn}^{(5)} + \sqrt{\omega\epsilon_0\beta_{zmn}^{(5)}\frac{(b-a)}{4}d\left[\left(\frac{m\cdot\pi}{b-a}\right)^2+\left(\frac{n\cdot\pi}{d}\right)^2\right]}. \tag{A16}$$

For the dielectric waveguide, the power is calculated numerically

$$P = \int_{x=a}^{x=b}\int_{y=0}^{y=d}(\vec E\times\vec H^*)\cdot\vec e_z\,dy\,dx. \tag{A17}$$

The normalization coefficient is then given by

$$N_\Psi = \pm h_\Psi\sqrt{P}. \tag{A18}$$

The following abbreviations have been used:

$$k_\nu^{CA} = \frac{1}{\epsilon_r^{(3)}}\cdot\frac{\cos\left[\beta_{y\nu}^{(2)}(h-d)\right]}{\cos\left[\beta_{y\nu}^{(3)}h\right]} \qquad k_\mu^{DB} = \frac{\sin\left[\tilde\beta_{y\mu}^{(2)}(h-d)\right]}{\sin\left[\tilde\beta_{y\mu}^{(3)}h\right]}$$

$$R_{k\nu} = \epsilon_r^{(3)}k_\nu^{CA}\int_{y=0}^{h}\cos\left(\beta_{y\nu}^{(3)}y\right)\cos\left(\frac{k\pi}{d}y\right)dy + \int_{y=h}^{d}\cos\left(\beta_{y\nu}^{(2)}(y-d)\right)\cos\left(\frac{k\pi}{d}y\right)dy$$

$$S_{k\mu} = k_\mu^{DB}\tilde\beta_{y\mu}^{(3)}\int_{y=0}^{h}\cos\left(\tilde\beta_{y\mu}^{(3)}y\right)\cos\left(\frac{k\pi}{d}y\right)dy + \tilde\beta_{y\mu}^{(2)}\int_{y=h}^{d}\cos\left(\tilde\beta_{y\mu}^{(2)}(y-d)\right)\cos\left(\frac{k\pi}{d}y\right)dy$$

$$Q_{k\mu} = k_\mu^{DB}\int_{y=0}^{h}\sin\left(\tilde\beta_{y\mu}^{(3)}y\right)\sin\left(\frac{k\pi}{d}y\right)dy + \int_{y=h}^{d}\sin\left(\tilde\beta_{y\mu}^{(2)}(y-d)\right)\sin\left(\frac{k\pi}{d}y\right)dy$$

$$P_{k\nu} = k_\nu^{CA}\beta_{y\nu}^{(3)}\int_{y=0}^{h}\sin\left(\beta_{y\nu}^{(3)}y\right)\sin\left(\frac{k\pi}{d}y\right)dy + \beta_{y\nu}^{(2)}\int_{y=h}^{d}\sin\left(\beta_{y\nu}^{(2)}(y-d)\right)\sin\left(\frac{k\pi}{d}y\right)dy$$

$$T_{k\nu} = k_\nu^{CA}\int_{y=0}^{h}\cos\left(\beta_{y\nu}^{(3)}y\right)\cos\left(\frac{k\pi}{d}y\right)dy + \int_{y=h}^{d}\cos\left(\beta_{y\nu}^{(2)}(y-d)\right)\cos\left(\frac{k\pi}{d}y\right)dy.$$

### E. Matrix (W) of the Waveamplitude Coefficients in (5)

$$(W) = \begin{pmatrix}(-HYL_{mn}) & (-HYP_{mn}) & (+HYH_{mn\Psi})\\ (-HXL_{mn}) & (-HXP_{mn}) & (+HXE+HXH)_{mn\Psi}\\ (-EYL_{mn}) & (+EYP_{mn}) & (+EYE_{mn\Psi})\\ (-EXL_{mn}) & (+EXP_{mn}) & (+EXE-EXH)_{mn\Psi}\end{pmatrix}^{-1}\cdot\begin{pmatrix}(-HYL_{mn}) & (+HYP_{mn}) & (-HYH_{mn\Psi})\\ (-HXL_{mn}) & (+HXP_{mn}) & (+HXE-HXH)_{mn\Psi}\\ (+EYL_{mn}) & (+EYP_{mn}) & (-EYE_{mn\Psi})\\ (+EXL_{mn}) & (+EXP_{mn}) & (-EXE-EXH)_{mn\Psi}\end{pmatrix}. \tag{A19}$$

*F. Matrix Elements in (A19)*

$$EXL_{mn} = j\cdot\omega\cdot\mu_0\cdot\frac{n\cdot\pi}{2}\cdot\frac{(b-a)}{2}\cdot N_m$$

$$EXP_{mn} = j\cdot\beta_{zmn}^{(5)}\cdot\frac{m\cdot\pi}{2}\cdot\frac{d}{2}$$

$$HXL_{mn} = j\cdot\beta_{zmn}^{(5)}\cdot\frac{m\cdot\pi}{2}\cdot\frac{d}{2}\cdot N_n$$

$$HXP_{mn} = j\cdot\omega\cdot\epsilon_0\cdot\frac{n\cdot\pi}{2}\cdot\frac{b-a}{2}$$

$$EYL_{mn} = -j\cdot\omega\cdot\mu_0\cdot\frac{m\cdot\pi}{2}\cdot\frac{d}{2}\cdot N_n$$

$$EYP_{mn} = j\cdot\beta_{zmn}^{(5)}\cdot\frac{n\cdot\pi}{2}\cdot\frac{b-a}{2}$$

$$HYL_{mn} = j\cdot\beta_{zmn}^{(5)}\cdot\frac{n\cdot\pi}{2}\cdot\frac{b-a}{2}\cdot N_m$$

$$HYP_{mn} = -j\cdot\omega\cdot\epsilon_0\cdot\frac{m\cdot\pi}{2}\cdot\frac{d}{2}. \tag{A20}$$

$$\begin{aligned}EXE_{mn\Psi} = &-E_{\Psi n}\cdot\beta_{x\Psi n}^{(4)}\cdot\frac{n\cdot\pi}{2}\cdot CINZ06_{\Psi mn}\\ &+\sum_{\nu=1}^{N+1}\left(A_{\Psi\nu}\cdot CINZ47_{\Psi\nu m}-A'_{\Psi\nu}\cdot CINZ48_{\Psi\nu m}\right)\\ &\cdot\beta_{x\Psi\nu}^{(2)}\cdot\beta_{y\Psi\nu}^{(2)}\cdot CINZ40_{\Psi_{\nu n}}\\ &+\sum_{\nu=1}^{N+1}\left(A_{\Psi\nu}\cdot CINZ47_{\Psi\nu m}-A'_{\Psi\nu}\cdot CINZ48_{\Psi_{\nu m}}\right)\\ &\cdot\beta_{x\Psi\nu}^{(2)}\cdot\beta_{y\Psi\nu}^{(3)}\cdot k_\nu^{CA}\cdot CINZ49_{\Psi\nu n}\\ &+G_{\Psi n}\cdot\beta_{x\Psi n}^{(4)}\cdot\frac{n\cdot\pi}{2}\cdot CINZ01_{\Psi mn}\end{aligned} \tag{A21}$$

$$\begin{aligned}EXH_{mn\Psi} = &\,\omega\cdot\mu_0\cdot F_{\Psi n}\cdot(-j\gamma_{z\Psi})\cdot\frac{d}{2}\cdot CINZ06_{\Psi mn}\\ &+\sum_{\mu=1}^{N}\left(B_{\Psi\mu}\cdot CINZ02_{\Psi\mu m}+B'_{\Psi\mu}\cdot CINZ03_{\Psi\mu m}\right)\\ &\cdot(-j\gamma_{z\Psi})\cdot CINZ05_{\Psi\mu n}\\ &+\sum_{\mu=1}^{N}\left(B_{\Psi\mu}\cdot CINZ02_{\Psi\mu m}+B'_{\Psi\mu}\cdot CINZ03_{\Psi\mu m}\right)\\ &\cdot(-j\gamma_{z\Psi})\cdot k_\mu^{DB}\cdot CINZ04_{\Psi\mu n}\\ &+H_{\Psi\mu}(-j\gamma_{z\Psi})\cdot\frac{d}{2}\cdot CINZ01_{\Psi mn}\end{aligned} \tag{A22}$$

$$\begin{aligned}HXE_{mn\Psi} = &\,\omega\cdot\epsilon_0\cdot E_{\Psi n}\cdot(-j\gamma_{z\Psi})\cdot\frac{d}{2}\cdot N_n\cdot CINZ16_{\Psi mn}\\ &+\sum_{\nu=1}^{N+1}\left(A_{\Psi\nu}\cdot CINZ17_{\Psi\nu m}+A'_{\Psi\nu}\cdot CINZ18_{\Psi\nu m}\right)\\ &\cdot(-j\gamma_{z\Psi})\cdot CINZ10_{\Psi\nu n}\\ &+\sum_{\nu=1}^{N+1}\left(A_{\Psi\nu}\cdot CINZ17_{\Psi\nu m}+A'_{\Psi\nu}\cdot CINZ18_{\Psi\nu m}\right)\\ &\cdot\epsilon_r^{(3)}\cdot k_\nu^{CA}\cdot CINZ19_{\Psi\nu n}\\ &+G_{\Psi n}\cdot\left(-j\gamma_{z\Psi}\frac{d}{2}\right)N_n\cdot CINZ11_{\Psi mn}\end{aligned} \tag{A23}$$

$$\begin{aligned}HXH_{mn\Psi} = &-F_{\Psi n}\cdot\beta_{x\Psi n}^{(4)}\cdot\frac{n\cdot\pi}{2}\cdot N_n\cdot CINZ16_{\Psi mn}\\ &+\sum_{\mu=1}^{N}\left(B_{\Psi\mu}\cdot CINZ12_{\Psi\mu m}-B'_{\Psi\mu}\cdot CINZ13_{\Psi\mu m}\right)\\ &\cdot\beta_{x\Psi\mu}^{(2)}\cdot\beta_{y\Psi\mu}^{(2)}\cdot CINZ15_{\Psi\mu n}\\ &+\sum_{\mu=1}^{N}\left(B_{\Psi\mu}\cdot CINZ12_{\Psi\mu m}-B'_{\Psi\mu}\cdot CINZ13_{\Psi\mu m}\right)\\ &\cdot\beta_{x\Psi\mu}^{(2)}\cdot\beta_{y\Psi\mu}^{(3)}\cdot k_\mu^{DB}\cdot CINZ14_{\Psi\mu n}\\ &+H_{\Psi n}\cdot\beta_{x\Psi n}^{(4)}\cdot\frac{n\cdot\pi}{2}\cdot N_n\cdot CINZ11_{\Psi mn}\end{aligned} \tag{A24}$$

$$\begin{aligned}EYE_{mn\Psi} = &\,E_{\Psi n}\cdot\left[\beta_{x\Psi n}^{(4)^2}-\gamma_{z\Psi}^2\right]\cdot\frac{d}{2}\cdot N_n\cdot CINZ16_{\Psi mn}\\ &+\sum_{\nu=1}^{N+1}\left(A_{\Psi\nu}\cdot CINZ17_{\Psi\nu m}+A'_{\Psi\nu}\cdot CINZ18_{\Psi\nu m}\right)\\ &\cdot\left[\beta_{x\Psi\nu}^{(2)^2}-\gamma_{z\Psi}^2\right]\cdot CINZ10_{\Psi\nu n}\\ &+\sum_{\nu=1}^{N+1}\left(A_{\Psi\nu}\cdot CINZ17_{\Psi\nu m}+A'_{\Psi\nu}\cdot CINZ18_{\Psi\nu m}\right)\\ &\cdot\left[\beta_{x\Psi\nu}^{(2)^2}-\gamma_{z\Psi}^2\right]\cdot k_\nu^{CA}\cdot CINZ19_{\Psi n}\\ &+G_{\Psi n}\cdot\left[\beta_{x\Psi n}^{(4)^2}-\gamma_{z\Psi}^2\right]\cdot\frac{d}{2}\cdot N_n\cdot CINZ11_{\Psi mn}\end{aligned} \tag{A25}$$

$$\begin{aligned}HYH_{mn\Psi} = &\,F_{\Psi n}\cdot\left[\beta_{x\Psi n}^{(4)^2}-\gamma_{z\Psi}^2\right]\cdot\frac{d}{2}\cdot CINZ06_{\Psi mn}\\ &+\sum_{\mu=1}^{N}\left(B_{\Psi\mu}\cdot CINZ02_{\Psi\mu m}+B'_{\Psi\mu}\cdot CINZ03_{\Psi\mu m}\right)\\ &\cdot\left[\beta_{x\Psi\mu}^{(2)^2}-\gamma_{z\Psi}^2\right]\cdot CINZ05_{\Psi\mu n}\\ &+\sum_{\mu=1}^{N}\left(B_{\Psi\mu}\cdot CINZ02_{\Psi\mu m}+B'_{\Psi\mu}\cdot CINZ03_{\Psi\mu m}\right)\\ &\cdot\left[\beta_{x\Psi\mu}^{(2)^2}-\gamma_{z\Psi}^2\right]\cdot k_\mu^{DB}\cdot CINZ04_{\Psi\mu n}\\ &+H_{\Psi n}\cdot\left[\beta_{x\Psi n}^{(4)^2}-\gamma_{z\Psi}^2\right]\cdot\frac{d}{2}\cdot CINZ01_{\Psi mn}.\end{aligned} \tag{A26}$$

*G. The Coupling Integrals in (A21)–(A26) Solved Analytically*

$$\begin{aligned}CINZ01_{\Psi mn} &= \int_{x=w}^{b}\cos\left(\beta_{x\Psi n}^{(4)}\cdot(x-b)\right)\\ &\quad\cdot\cos\left(\frac{m\pi}{b-a}(x-a)\right)\cdot dx\\ CINZ02_{\Psi\mu m} &= \int_{x=-w}^{+w}\cos\left(\beta_{x\Psi\mu}^{(2)}\cdot x\right)\cdot\cos\left(\frac{m\pi}{b-a}(x-a)\right)\cdot dx\\ CINZ03_{\Psi\mu m} &= \int_{x=-w}^{+w}\sin\left(\tilde\beta_{x\Psi\mu}^{(2)}\cdot x\right)\cdot\cos\left(\frac{m\pi}{b-a}(x-a)\right)\cdot dx\\ CINZ04_{\Psi\mu n} &= \int_{y=0}^{h}\sin\left(\tilde\beta_{y\Psi\mu}^{(3)}\cdot y\right)\cdot\sin\left(\frac{n\pi}{d}y\right)\cdot dy\\ CINZ05_{\Psi\mu n} &= \int_{y=h}^{d}\sin\left(\tilde\beta_{y\Psi\mu}^{(2)}\cdot(y-d)\right)\cdot\sin\left(\frac{n\pi}{d}y\right)\cdot dy\\ CINZ06_{\Psi mn} &= \int_{x=a}^{-w}\cos\left(\beta_{x\Psi n}^{(4)}\cdot(x-a)\right)\\ &\quad\cdot\cos\left(\frac{m\pi}{b-a}(x-a)\right)\cdot dx.\end{aligned} \tag{A27}$$

$$CINZ10_{\Psi\nu n} = \int_{y=h}^{d} \cos\left(\beta^{(2)}_{y\Psi_\nu}\cdot(y-d)\right)\cdot\cos\left(\frac{n\pi}{d}y\right)\cdot dy$$

$$CINZ11_{\Psi mn} = \int_{x=a}^{-w} \sin\left(\beta^{(4)}_{x\Psi_n}\cdot(x-b)\right) \cdot\sin\left(\frac{m\pi}{b-a}(x-a)\right)\cdot dx$$

$$CINZ12_{\Psi\mu m} = \int_{x=-w}^{+w} \sin\left(\tilde{\beta}^{(2)}_{x\Psi_\mu}\cdot x\right)\cdot\sin\left(\frac{m\pi}{b-a}(x-a)\right)\cdot dx$$

$$CINZ13_{\Psi\mu m} = \int_{x=-w}^{+w} \cos\left(\tilde{\beta}^{(2)}_{x\Psi_\mu}\cdot x\right)\cdot\sin\left(\frac{m\pi}{b-a}(x-a)\right)\cdot dx$$

$$CINZ14_{\Psi\mu n} = \int_{y=0}^{h} \cos\left(\tilde{\beta}^{(3)}_{y\Psi_\mu}\cdot y\right)\cdot\cos\left(\frac{n\pi}{d}y\right)\cdot dy$$

$$CINZ15_{\Psi\mu n} = \int_{y=h}^{d} \cos\left(\tilde{\beta}^{(2)}_{y\Psi_\mu}\cdot(y-d)\right)\cdot\cos\left(\frac{n\pi}{d}y\right)\cdot dy$$

$$CINZ16_{\Psi mn} = \int_{x=a}^{-w} \sin\left(\beta^{(4)}_{x\Psi_n}\cdot(x-a)\right) \cdot\sin\left(\frac{m\pi}{b-a}(x-a)\right)\cdot dx$$

$$CINZ17_{\Psi\nu m} = \int_{x=-w}^{+w} \sin\left(\beta^{(2)}_{x\Psi_\nu}\cdot x\right)\cdot\sin\left(\frac{m\pi}{b-a}(x-a)\right)\cdot dx$$

$$CINZ18_{\Psi\nu m} = \int_{x=-w}^{+w} \cos\left(\beta^{(2)}_{x\Psi_\nu}\cdot x\right)\cdot\sin\left(\frac{m\pi}{b-a}(x-a)\right)\cdot dx$$

$$CINZ19_{\Psi\nu n} = \int_{y=0}^{h} \cos\left(\beta^{(3)}_{y\Psi_\nu}\cdot y\right)\cdot\cos\left(\frac{n\pi}{d}y\right)\cdot dy. \qquad \text{(A28)}$$

$$CINZ40_{\Psi\nu n} = \int_{y=h}^{d} \sin\left(\beta^{(2)}_{y\Psi_\nu}\cdot(y-d)\right)\cdot\sin\left(\frac{n\pi}{d}y\right)\cdot dy$$

$$CINZ47_{\Psi\nu m} = \int_{x=-w}^{+w} \cos\left(\beta^{(2)}_{x\Psi_\nu}\cdot x\right)\cdot\cos\left(\frac{m\pi}{b-a}(x-a)\right)\cdot dx$$

$$CINZ48_{\Psi\nu m} = \int_{x=-w}^{+w} \sin\left(\beta^{(2)}_{x\Psi_\nu}\cdot x\right)\cdot\cos\left(\frac{m\pi}{b-a}(x-a)\right)\cdot dx$$

$$CINZ49_{\Psi\nu n} = \int_{y=0}^{h} \sin\left(\beta^{(3)}_{y\Psi_\nu}\cdot y\right)\cdot\sin\left(\frac{n\pi}{d}y\right)\cdot dy. \qquad \text{(A29)}$$

## REFERENCES


[1] D. D. King, "Circuit components in dielectric image lines," *IRE Trans. Microwave Theory Tech.*, vol. MTT-3, pp. 35–39, Dec. 1955.

[2] E. A. J. Marcatili, "Dielectric rectangular waveguide and directional coupler for integrated optics," *Bell Syst. Tech. J.*, vol. 48, pp. 2071–2102, Sept. 1969.

[3] W. V. McLevidge, T. Itoh, and R. Mittra, "New waveguide structures for millimeter-wave and optical integrated circuits," *IEEE Trans. Microwave Theory Tech.*, vol. MTT-23, pp. 788–794, Oct. 1975.

[4] R. M. Knox, "Dielectric waveguide microwave integrated circuits—An overview," *IEEE Trans. Microwave Theory Tech.*, vol. MTT-24, pp. 806–814, Nov. 1976.

[5] T. Itoh, "Application of gratings in a dielectric waveguide for leaky-wave antennas and band-reject filters," *IEEE Trans. Microwave Theory Tech.*, vol. MTT-25, pp. 1134–1138, Dec. 1977.

[6] J. A. Paul and Y.-W. Chang, "Millimeter wave image-guide integrated passive devices," *IEEE Trans. Microwave Theory Tech.*, vol. MTT-26, pp. 751–754, Oct. 1978.

[7] K. Solbach, "Electric probe measurements on dielectric image lines in the frequency range of 26–90 GHz," *IEEE Trans. Microwave Theory Tech.*, vol. MTT-26, pp. 755–758, Oct. 1978.

[8] K. Solbach, "The calculation and the measurements of the coupling properties of dielectric image lines of rectangular cross section," *IEEE Trans. Microwave Theory Tech.*, vol. MTT-27, pp. 54–58, Jan. 1979.

[9] J. A. Paul and P. C. H. Yen, "Millimeter-wave passive components and six-port network analyzer in dielectric waveguide," *IEEE Trans Microwave Theory Tech.*, vol. MTT-29, pp. 948–953, Sept. 1981.

[10] T. Itoh, "Open guiding structures for mmW integrated circuits," *Microwave J.*, pp. 113–126, Sept. 1982.

[11] R. K. Winn and J. K. Harris, "Coupling from multimode to single-mode linear waveguides using horn-shaped structures," *IEEE Trans. Microwave Theory Tech.*, vol. MTT-23, pp. 92–97, Jan. 1975.

[12] G. L. Matthaei, "A note concerning modes in dielectric waveguide gratings for filter applications," *IEEE Trans. Microwave Theory Tech.*, vol. MTT-31, pp. 309–312, Mar. 1983.

[13] G. L. Matthaei, D. C. Park, Y. M. Kim, and D. L. Johnson, "A study of the filter properties of single and parallel-coupled dielectric-waveguide gratings," *IEEE Trans Microwave Theory Tech.*, vol. MTT-31, pp. 825–835, Oct 1983.

[14] K. Webb and R. Mittra, "Dielectric waveguide grating filter," *Arch. Elek. Übertragung.*, vol. 38, pp. 51–54, Jan. 1984.

[15] W. O. Schlosser, "Der rechteckige dielektrische Draht," *Arch. Elek. Übertragung.*, vol. 18, pp. 403–409, 1964.

[16] W. O. Schlosser and H. G. Unger, "Partially filled waveguides and surface waveguides of rectangular cross section," in *Advances in Microwaves*, Vol. 1. New York: Academic Press, 1966, pp. 319–387.

[17] K. Solbach and I. Wolff, "The electromagnetic fields and the phase constants of dielectric image lines," *IEEE Trans. Microwave Theory Tech.*, vol. MTT-26, pp. 266–274, Apr. 1978.

[18] N. Deo and R. Mittra, "A technique for analyzing planar dielectric waveguides for millimeter wave integrated circuits," *Arch. Elek. Übertragung.*, vol. 37, pp. 236–244, July/August 1983.

[19] T. E. Rozzi and G. H. In't Veld, "Field and network analysis of interacting step discontinuities in planar dielectric waveguides," *IEEE Trans. Microwave Theory Tech.*, vol. MTT-27, pp. 303–309, Apr. 1979.

[20] A. A. Oliner, S.-T. Peng, T.-I. Hsu, and A. Sanchez, "Guidance and leakage properties of a class of open dielectric waveguides: Part II —New physical effects," *IEEE Trans. Microwave Theory Tech.*, vol. MTT-29, pp. 855–869, Sept. 1981.

[21] P. J. B. Clarricoats and K. R. Slinn, "Complex modes of propagation in dielectric loaded circular waveguide," *Electron. Lett.*, vol. 1, pp. 145–146, 1965.

[22] V. A. Kalmyk, S. B. Rayevskiy, and V. P. Ygvyumov, "An experimental verification of existence of complex waves in a two-layer, circular, shielded waveguide," *Radio Eng. Electron. Phys*, vol. 23, pp. 16–19, 1978.

[23] J. Strube and F. Arndt, "Three-dimensional higher-order mode analysis of transition from waveguide to shielded dielectric image line," *Electron. Lett.*, vol. 19, pp. 306–307, Apr. 1983.

[24] U. Crombach, "Complex waves on shielded lossless rectangular dielectric image guide," *Electron. Lett.*, vol. 19, pp. 557–558, July 1983.

[25] H. Katzier and F. J. K. Lange, "Grundlegende Eigenschaften komplexer Wellen am Beispiel der geschirmten kreiszylindrischen dielektrischen Leitung," *Arch. Elek. Übertragung.*, vol. 37, pp. 1–5, Jan./Feb. 1983.

[26] R. E. Collin, *Field Theory of Guided Waves*. New York: McGraw-Hill, 1960, ch. 1.6.

[27] K. Solbach and I. Wolff, "Integrierte Millimeter-wellenschaltungen," 2nd Research Rep., University of Duisburg, Germany.

[28] J. Strube, "Berechnung des Wellenverhaltens am abrupten Übergang vom Rechteckhohlleiter zum geschirmten dielektrischen Wellenleiter mit der Methode der Orthogonalentwicklung," Dr.-Ing. thesis, University of Bremen, June 1983; also appeared in *Fortschritt-Berichte*. Düsseldorf: VDI-Verlag, vol. 9, no. 39, 1983

[29] R. F. Harrington, *Time-Harmonic Electromagnetic Fields*. New York: McGraw-Hill, 1961, ch. 2.7.

[30] H. Schmiedel, "Anwendung der Evolutionsoptimierung bei Mikrowellenschaltungen," *Frequenz*, vol. 35, pp. 306–310, Nov. 1980.

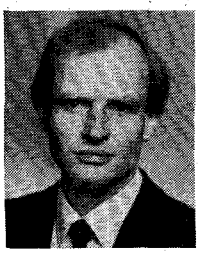

**Jürgen Strube** received the Dipl.-Ing. and Dr.-Ing. degrees, both in electrical engineering, from the University of Bremen, Germany, in 1975 and 1983, respectively.

In August 1975, he joined the ERNO Raumfahrttechnik GmbH at Bremen, Germany, as a Systems Engineer. He was involved in the design, development, and testing of the Spacelab, the European contribution to the Space Shuttle Project. Since 1979, he has been with the University of Bremen as a Research Associate and is working on various dielectric waveguide structures.

♣

**Fritz Arndt** (SM'83) was born in Konstanz, Germany, on April 30, 1938. He received the Dipl.-Ing., the Dr.-Ing., and the Habilitation degrees from the Technical University of Darmstadt, Germany, in 1963, 1968, and 1972, respectively.

From 1963 to 1972, he worked on directional couplers and microstrip techniques at the Technical University of Darmstadt. Since 1972, he has been a Professor and Head of the Microwave Department at the University of Bremen, Germany. His research activities are at present in the area of the solution of field problems of waveguide, finline, and optical waveguide structures, of antenna design, and of scattering structures.

Dr. Arndt is member of the VDE and NTG (Germany). In 1970, he received the NTG award, and in 1982, the A.F. Bulgin Award (together with three coauthors) from the Institution of Radio and Electronic Engineers.